Stopped-flow kinetic studies of electron transfer in the reductase domain of neuronal nitric oxide synthase: re-evaluation of the kinetic mechanism reveals new enzyme intermediates and variation with cytochrome P450 reductase

Kirsty KNIGHT and Nigel S. SCRUTTON[1]

Department of Biochemistry, University of Leicester, University Road, Leicester LE1 7RH, U.K.

The reduction by NADPH of the FAD and FMN redox centres in the isolated flavin reductase domain of calmodulin-bound rat neuronal nitric oxide synthase (nNOS) has been studied by anaerobic stopped-flow spectroscopy using absorption and fluorescence detection. We show by global analysis of time-dependent photodiode array spectra, single wavelength absorption and NADPH fluorescence studies, that at least four resolvable steps are observed in stopped-flow studies with NADPH and that flavin reduction is reversible. The first reductive step represents the rapid formation of an equilibrium between an NADPH-enzyme charge-transfer species and two-electron-reduced enzyme bound to $NADP^+$. The second and third steps represent further reduction of the enzyme flavins and $NADP^+$ release. The fourth step is attributed to the slow accumulation of an enzyme species that is inferred not to be relevant catalytically in steady-state reactions. Stopped-flow flavin fluorescence studies indicate the presence of slow kinetic phases, the timescales of which correspond to the slow phase observed in absorption and NADPH fluorescence transients. By analogy with stopped-flow studies of cytochrome P450 reductase, we attribute these slow fluorescence and absorption changes to enzyme disproportionation and/or conformational change. Unlike for the functionally related cytochrome P450 reductase, transfer of the first hydride equivalent from NADPH to nNOS reductase does not generate the flavin di-semiquinoid state. This indicates that internal electron transfer is relatively slow and is probably gated by $NADP^+$ release. Release of calmodulin from the nNOS reductase does not affect the kinetics of inter-flavin electron transfer under stopped-flow conditions, although the observed rate of formation of the equilibrium between the NADPH-oxidized enzyme charge-transfer species and two-electron-reduced enzyme bound to $NADP^+$ is modestly slower in calmodulin-depleted enzyme. Our studies indicate the need for significant re-interpretation of published kinetic data for electron transfer in the reductase domain of neuronal nitric oxide synthase.

Key words: calmodulin, flavoprotein, transient kinetics.

INTRODUCTION

The nitric oxide synthase (NOS) isoforms catalyse the NADPH- and oxygen-dependent conversion of L-arginine to L-citrulline and nitric oxide [1–3]. They are dimeric flavohaem enzymes: each monomer comprises a C-terminal diflavin reductase domain and an N-terminal oxygenase domain [4–7]. The reductase domain contains one mole equivalent of FAD and FMN, binds NADPH and is related structurally and functionally to cytochrome P450 reductase (CPR) [8,9], methionine synthase reductase ('MSR' [10]) and protein NR1 [11]. The N-terminal oxygenase domain of NOS contains one mole equivalent of haem and possesses binding sites for L-arginine and (6*R*)-5,6,7,8-tetrahydrobiopterin (BH_4 [12]). The reductase and oxygenase domains are linked by a calmodulin (CaM) binding sequence [8,13,14]; CaM binding facilitates electron transfer from the reductase to the oxygenase domain [15] and is proposed also to enhance the rate of interflavin electron transfer [16–18]. Of the three NOS isoforms, the inducible NOS (iNOS) isoform is expressed with CaM tightly bound [13] and regulation of activity is primarily through transcriptional processes; the activities of endothelial NOS (eNOS) and neuronal NOS (nNOS) are regulated by CaM binding, which in turn is controlled by intracellular calcium levels [4,5,7] and is mediated by an autoinhibitory sequence in the FMN domain [19].

The oxygenase domain of the NOS isoforms receives electrons from the reductase domain in a mechanism similar to that catalysed by CPR and the cytochrome P450 enzymes. Unlike with NOS, however, the cytochrome P450 enzymes are distinct entities that are not covalently linked to the reductase module. CPR and the NOS reductase domain have common functional properties: both transfer electrons to several different artificial acceptors such as cytochrome *c*, dichlorophenolindophenol, and ferricyanide [14,16,20] and the redox potentials of the flavin couples are similar for each enzyme [21,22]. Also, like CPR, the NOS reductase domain must be reduced beyond a one-electron-reduced state to enable efficient electron transfer to the oxygenase domain [23,24]. Of the mammalian diflavin enzymes, stopped-flow and steady-state kinetic studies of CPR are perhaps the most advanced [25–28]. Detailed mechanisms for electron flow and the effects of ligand binding and ionic strength have been reported [29,30]. Studies with NOS have focused on thermodynamic and rapid kinetic approaches with the aim of establishing the mechanism of electron flow, the role of bound

Abbreviations used: BH_4, (6*R*)-5,6,7,8-tetrahydro-L-biopterin; CaM, calmodulin; CPR, cytochrome P450 reductase; NOS, nitric oxide synthase; eNOS, endothelial NOS; FAD_{hq}, hydroquinone FAD; FAD_{sq} semiquinone FAD; FMN_{ox}, oxidized FMN; FMN_{sq}, semiquinone FMN; iNOS, inducible NOS; nNOS, neuronal NOS; nNOS CaM^+, nNOS reductase complexed with CaM; nNOS CaM^-, nNOS reductase in which CaM has been removed by treatment with EDTA.

[1] To whom correspondence should be addressed (e-mail nss4@le.ac.uk).

CaM, and any mechanistic equivalence with CPR. CaM binding does not perturb the redox potentials of the flavin couples in nNOS reductase [22], but is proposed to enhance the rates of electron transfer through the reductase domain [16–18] and to the oxygenase domain [15]. Moreover, flavin to haem electron transfer is suggested to be rate-limiting on the basis of stopped-flow studies of the three NOS isoforms [24].

In this paper we have performed detailed stopped-flow studies of electron transfer in CaM-bound and CaM-depleted nNOS reductase domain under anaerobic conditions using absorption and fluorescence detection. We show that previous stopped-flow studies of electron transfer in NOS, which have relied entirely on absorption detection, have not accounted for additional kinetic phases in the reductive half-reaction. This has led to the over-simplification of kinetic phases and the construction of inappropriate kinetic models. Consequently, the role of CaM in facilitating electron transfer in the reductase domain needs to be re-evaluated. We show in this paper that bound CaM does not enhance the rate of interflavin electron transfer in stopped-flow studies with isolated nNOS reductase, although there is a very modest effect on the rate of formation of the equilibrium between an NADPH-enzyme charge-transfer species and two electron-reduced enzyme bound to $NADP^+$. We show that interflavin electron transfer is relatively slow in nNOS reductase and is probably gated by $NADP^+$-release. The blue di-semiquinoid species (a prominent intermediate in the CPR reaction [25,27]) does not accumulate in stopped-flow studies with NOS, despite its formation in equilibrium titration experiments. Our data reveal that the mechanism of electron transfer in nNOS reductase needs to be re-evaluated. On the basis of our data, we present a new kinetic scheme to explain the mechanism of electron transfer in the reductase domain of nNOS.

EXPERIMENTAL PROCEDURES

Protein purification

The plasmid pCRNNR encoding rat nNOS reductase was supplied by Dr J. G. Guillemette (Department of Biochemistry, University of Waterloo, Ontario, Canada). *E. coli* strain JM109 transformed with plasmid pCRNNR was grown (12×2 litre flasks containing 500 ml media each) in 'terrific broth' (containing 12 g/l bactotryptone, 24 g/l yeast extract, 4 ml/l glycerol, 0.72 M K_2HPO_4, 0.17 M KH_2PO_4) supplemented with ampicillin (100 μg/ml). Expression of nNOS reductase was induced by the addition of isopropyl β-D-thiogalactoside (1 mM) at a culture attenuance of 0.8 at 600 nm; cells were grown for a further 24 h at 30 °C. Harvested cells were resuspended in 50 ml of lysis buffer [50 mM Tris/HCl, pH 7.4, containing 10 % (v/v) glycerol, 1 mM $CaCl_2$ and a Complete™ EDTA-free protease inhibitor tablet (Roche)]. Cells were disrupted by sonication, the cell extract clarified by centrifugation (15000 ***g***, 50 min) and fractionated with ammonium sulphate (nNOS reductase was recovered in the 30–50 % saturation fraction). Enzyme was dialysed exhaustively against lysis buffer, and applied to an anion-exchange resin (DE-52) previously equilibrated with lysis buffer. The column was washed with lysis buffer (500 ml) and nNOS reductase was recovered by developing the column with a gradient (0–0.5 M) of KCl. Fractions containing nNOS reductase were pooled, and applied to an affinity-resin (2′5′-ADP Sepharose) equilibrated with lysis buffer containing 100 mM NaCl. After washing ($\approx$ 250 ml lysis buffer containing 100 mM NaCl, followed by $\approx$ 250 ml lysis buffer containing 250 mM NaCl), nNOS reductase was recovered by the application of lysis buffer containing 500 mM NaCl. Enzyme was dialysed exhaustively against lysis buffer and stored at -20 °C in the presence of 20 % (v/v) glycerol. SDS/PAGE confirmed the presence of nNOS reductase (as a single unproteolysed band on the gel) and CaM (as an additional band). N-terminal sequence analysis confirmed the presence of the CaM-binding region in the purified nNOS reductase domain (residues 733–1429) and the lack of significant proteolysed material (as judged by the lack of secondary sequence during automated Edman degradation).

Purification of nNOS reductase in the absence of $CaCl_2$ resulted in the generation of a proteolysed form of nNOS reductase (residues 743–1429) that lacks the CaM-binding domain; consequently, the domain is not associated with CaM. Complete loss of residues 733 to 743 was confirmed by N-terminal sequence analysis. The absence of CaM and any unproteolysed nNOS reductase domain was also confirmed by SDS/PAGE. Removal of CaM from non-proteolysed nNOS reductase was achieved by the addition of EDTA (0.6 mM); the quenching of flavin fluorescence at 530 nm was used to follow the release of CaM from nNOS reductase [31]. The concentration of purified nNOS reductase was determined by absorption measurements at 455 nm ($\epsilon = 21600\ M^{-1} \cdot cm^{-1}$ [24]) based on two flavins per protein monomer. Flavin content and the absorption spectra of the purified nNOS reductase enzymes were as published previously [17]. In steady-state assays, the enzyme displayed the usual CaM-dependent stimulation of cytochrome *c* reductase activity and determined values of apparent K_m and k_{cat} were as published previously [31]. The enzyme was purified predominantly in the 'air-stable' semiquinone state; prior to all stopped-flow kinetic studies, nNOS reductase was oxidized with potassium hexacyanoferrate using the procedure reported in our recent work on human CPR [25]. Titration of oxidized enzyme to the two-electron level with NADPH generates the blue-semiquinone species of nNOS reductase, thus establishing that the enzyme, as purified, has identical properties to those reported by other workers.

Synthesis of A-side $NADP^2H$

A-side $NADP^2H$ was synthesized enzymically using a procedure similar to that described by Viola and coworkers [32]. [$^2H_6$]Ethanol (260 mM), $NADP^+$ (8 mM), *T brockii* alcohol dehydrogenase (35 units; supplied by Fluka, Gillingham, Dorset, U.K.), yeast aldehyde dehydrogenase (100 units; supplied by Calbiochem, Nottingham, U.K.) were mixed in 20 ml of 20 mM Taps buffer, pH 9.0. The reaction was maintained at pH 9 throughout the reaction and allowed to proceed to completion, as determined by absorbance measurements at 340 nm. Purification of A-side $NADP^2H$ by ethanol precipitation was by the method of Pollock and Barber [33]. A further purification step was performed using a Q-Sepharose column. The column was equilibrated with 10 mM ammonium hydrogen carbonate, pH 9 (buffer A) and the A-side $NADP^2H$ ($\approx$ 30 mg per chromatographic run) applied to the column. The column was washed with buffer A and then with 200 mM ammonium hydrogen carbonate, pH 9.0. A-side $NADP^2H$ was eluted from the column with 400 mM ammonium hydrogen carbonate. Nucleotide-containing fractions were freeze-dried and dissolved in 20 mM Taps buffer, pH 9.0, prior to use in kinetic experiments. The A_{260}/A_{340} ratio of the product was 1.9, consistent with pure preparations of A-side $NADP^2H$ obtained by other workers [33]. $NADP^2H$ synthesized by this method gives rise to the expected published primary kinetic isotope effect (KIE = 7.0; [34]) in stopped-flow reactions with pentaerythritol tetranitrate reductase and yields a monophasic transient for flavin reduction. NADPH synthesized in the same way does not produce inhibitory products in this same reaction and likewise yields a monophasic kinetic transient.

Kinetic measurements

Stopped-flow studies were performed using an Applied Photophysics SX.17 MV stopped-flow spectrophotometer. Unless otherwise stated, measurements were carried out at 25 °C in 50 mM Tris/HCl buffer (pH 7.4) containing 10 % (v/v) glycerol. For reactions performed with nNOS reductase complexed with CaM (nNOS CaM^+), $CaCl_2$ (1 mM) was included in the buffer. Protein concentration was 5 μM (reaction cell concentration), and reactions were performed under anaerobic conditions. For this purpose, the sample-handling unit of the stopped-flow instrument was contained within a glove box (Belle Technology, Portesham, Dorset, U.K.). All buffers were made oxygen-free by evacuation and extensive bubbling with argon before use. Buffers were then placed in the glove box overnight before use. Prior to stopped-flow studies, protein samples were treated with potassium hexacyanoferrate, and excess cyanoferrate was removed by rapid gel filtration [Sephadex G25 equilibrated in 50 mM Tris/HCl (pH 7.4), 10 % (v/v) glycerol and 1 mM $CaCl_2$].

Stopped-flow, multiple-wavelength absorption studies were carried out using a photodiode array detector and X-SCAN software (Applied Photophysics Ltd, Surrey, U.K.). Spectral deconvolution was performed by global analysis and numerical integration methods using PROKIN software (Applied Photophysics Ltd). In single wavelength studies, flavin reduction by NADPH was observed at 458 nm. Transients were triphasic (over 500 ms) and were fitted using the standard triple exponential expression eqn (1)

$$A_{450} = C_1 e^{-k_{obs1}t} + C_2 e^{-k_{obs2}t} + C_3 e^{-k_{obs3}t} + b \quad (1)$$

where k_{obs1}, k_{obs2} and k_{obs3} are the observed rate constants for the fast, intermediate and slow phases respectively, C_1, C_2 and C_3 are the relative amplitude values for the three phases, and b is an offset value to account for a non-zero baseline. Transients at 600 nm report on the appearance and decay of the initial enzyme–NADPH charge-transfer species and have a characteristic 'up' and 'down' phase. Truncated transients obtained with 10-fold excess NADPH were fitted approximately, using eqn (2) (see text for details):

$$A_{600} = \frac{k_{obs1}}{k_{obs2} - k_{obs1}} C(e^{-k_{obs1}t} - e^{-k_{obs2}t}) + b \quad (2)$$

where k_{obs1} and k_{obs2} are observed rate constants for the formation and decay of the charge-transfer intermediate respectively, C is the amplitude term and b an off-set value. Stopped-flow fluorescence experiments employed excitation wavelengths of 340 nm (NADPH) and 458 nm (flavin). Emission bands were selected using the appropriate band-pass filter [450 nm (#35-3367) and 520 nm (#35-5545) from Coherent Optics, Greycain Road, Watford, Herts., U.K.]. Data fitting to fluorescence transients was using standard biphasic or triphasic expressions (see Results section).

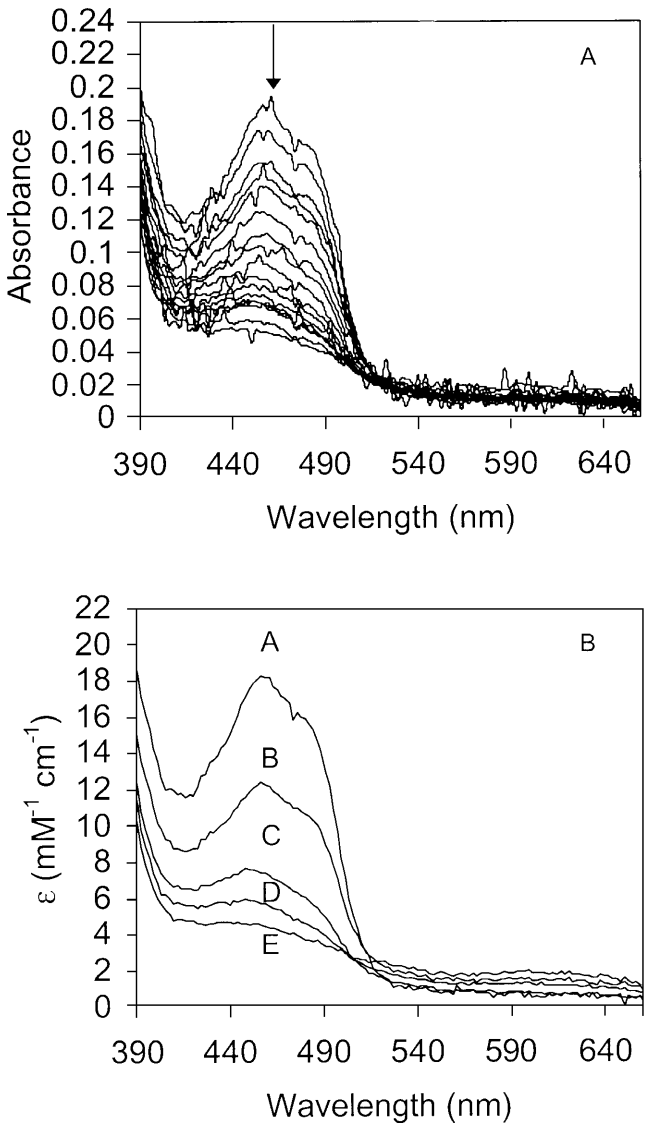

Figure 1 Reaction of nNOS CaM^+ with NADPH monitored by stopped-flow photodiode array spectroscopy

Conditions: 50 mM Tris/HCl buffer (pH 7.4), 10% (v/v) glycerol and 1 mM $CaCl_2$ at 25 °C. [nNOS CaM^+] = 9 μM; [NADPH] = 90 μM. (**A**) Time-dependent spectral changes on rapidly mixing nNOS CaM^+ with NADPH. The experiment was performed over 10 s after the initial mixing event. The first spectrum was recorded at 1.28 ms after mixing; for clarity only selected subsequent spectra are shown. The arrow indicates the direction of spectral change. (**B**) Deconvoluted spectra for the reaction shown in (**A**). The data in (**A**) were fitted to a reversible four-step model A → B → C → D → E. The rate constants (s^{-1}; obtained from global fitting) for this kinetic scheme are A → B, 210 ± 9; B → A, 4 ± 0.2; B → C, 30 ± 0.5; C → B, 6 ± 1; C → D, 11 ± 0.4; D → C, 0.04 ± 0.1; D → E, 0.3 ± 0.02; E → D, 0.03 ± 0.01.

RESULTS

Flavin reduction followed by photodiode array spectroscopy

The reductive half-reaction of the nNOS reductase domain (nNOS CaM^+) was initially studied at 25 °C under pseudo-first order conditions (10-fold excess NADPH) using photodiode array detection (Figure 1). The spectra as a function of time were fitted globally by numerical integration methods using Prokin software (Applied Photophysics). Data collected over a period of 10 s from the mixing event were best fitted to a four-step reversible model (A → B → C → D → E; Figure 1). Model validity was assessed using a number of criteria: the lack of systematic deviations of the residual plot; inspection of the calculated spectra to ensure they made chemical sense in terms of shape and sign; confirmation that the number of significant singular values following singular value decomposition was consistent with the fitted model. Data-fitting using simpler models (sequential three-step and two-step) was inadequate using these validity criteria, in that systematic deviations were seen in the residual plots,

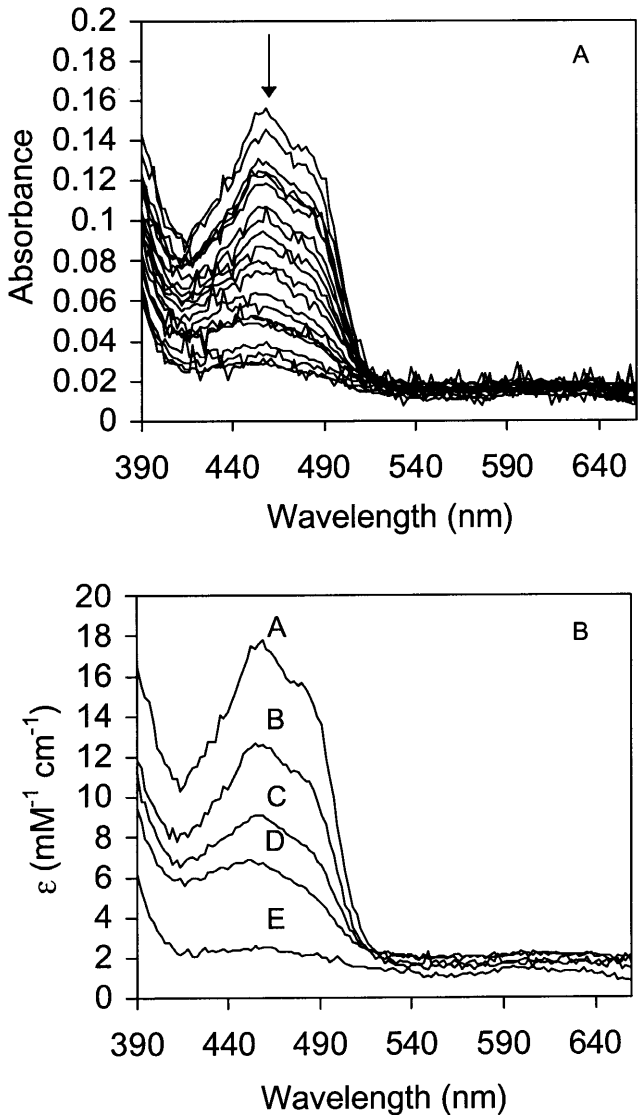

Figure 2 Reaction of the proteolysed form of nNOS reductase with NADPH monitored by stopped-flow photodiode array spectroscopy

Conditions: as for Figure 1. (**A**) Time-dependent spectral changes on rapidly mixing the proteolysed form of nNOS reductase with NADPH. The experiment was performed over 10 s after the initial mixing event. The first spectrum was recorded at 1.28 ms after mixing; for clarity only selected subsequent spectra are shown. The arrow indicates the direction of spectral change. (**B**) Deconvoluted spectra for the reaction shown in (**A**). The four-step model (Figure 1) was used in data fitting. The rate constants (s^{-1}; obtained from global fitting) for this kinetic scheme are A → B, 290 ± 10; B → A, 7 ± 0.3; B → C, 37 ± 0.5; C → B, 4 ± 0.3; C → D, 4 ± 0.3; D → C, 0.1 ± 0.06; D → E, 0.2 ± 0.01; E → D, 0.05 ± 0.01. Time-dependent spectral changes, and the calculated spectra of intermediates and rate constants for their formation, were similar for nNOS CaM^- (not shown).

indicating that spectral events had been missed. Also, using these simpler models, convergence was not obtained after 20 iterative cycles, unlike for the four-step reversible model, and some of the calculated spectra for the simpler models did not make chemical sense, in terms of the expected spectral properties of flavin. Corresponding studies were performed with nNOS reductase in which CaM has been removed by treatment with EDTA (nNOS CaM^-) and the proteolysed form of the reductase domain to assess the potential role of CaM in the mechanism of electron transfer in the reductase domain. Photodiode array analysis and global fitting of data revealed that the four-step model proposed for nNOS CaM^+ was equally valid for nNOS CaM^- and proteolysed reductase (Figure 2), and rate constants for formation and decay of reaction intermediates were found to be comparable. The final spectrum, E, for nNOS CaM^- and the proteolysed form of nNOS reductase were similar, but both differ from that seen with nNOS CaM^+ for reasons that are not clear (see below). In single wavelength studies (see below), the CaM-free form of nNOS reductase (nNOS CaM^-) generated by the addition of EDTA to nNOS CaM^+ was used for comparative studies with nNOS CaM^+. At this point it is important to emphasize that species A, B, C, D and E are spectral intermediates and not discrete enzyme intermediates. This arises because the electron transfer in nNOS reductase is reversible (see below) and each spectral intermediate comprises a number of different enzyme forms determined by the equilibrium distribution.

The challenge arising from fitting to a relatively complex (sequential four-step) model is identification of the intermediate and final enzyme species in the stopped-flow experiment. Identification of some of these species has come from the additional fluorescence and single wavelength absorption studies that are described below. A notable feature of the spectral changes observed for reactions of nNOS reductase with NADPH is the absence of appreciable signatures in the long wavelength region (600–650 nm) that occur during flavin reduction. The data indicate that a blue di-semiquinoid form of nNOS reductase domain, containing semiquinone FMN (FMN_{sq}) and semiqinone FAD (FAD_{sq}), does not accumulate at significant levels in the stopped-flow experiment, even though it forms under equilibrium conditions during titration experiments with NADPH [24]. This finding is in stark contrast to stopped-flow studies on CPR where, owing to the relatively fast rate of interflavin electron transfer in CPR [25], the di-semiquinoid species forms immediately following hydride transfer from NADPH to FAD. The inability to populate the blue di-semiquinoid form of NOS reductase suggests that there is a kinetic restriction on forming this intermediate. Potentiometric studies of nNOS reductase [22] have indicated that the redox potential of the oxidized FMN (FMN_{ox})/FMN_{sq} couple, like that of CPR [21], is substantially more positive than the other flavin couples in the domain, and thus should provide a strong driving force for electron transfer to the FMN [i.e. hydroquinone FAD (FAD_{hq})/FMN_{ox} → FAD_{sq}/FMN_{sq}]. As discussed below, the kinetic restriction that prevents formation of the blue semiquinone in stopped-flow experiments with nNOS reductase is attributed to the slow release of $NADP^+$ from reduced enzyme. In human CPR, $NADP^+$ release is relatively fast [25], allowing rapid internal electron transfer to form the blue di-semiquinoid intermediate. In the Trp^{676} → His mutant of CPR, $NADP^+$ release is impaired, and the blue di-semiquinoid intermediate does not form in stopped-flow studies, although it does accumulate under equilibrium titration conditions following reduction at the two-electron level with sodium dithionite or NADPH [26]. This situation is analogous to that seen with nNOS reductase.

Assignment of intermediates by single-wavelength absorption and fluorescence studies

Single-wavelength stopped-flow absorption and fluorescence studies were used to measure rate constants for the formation of spectral intermediates seen in the photodiode array experiments and also to provide evidence for the assignment of kinetic phases. In single-wavelength studies, rate constants determined by the fitting of transients are *observed* rate constants (i.e. they are the

sum of the rate constants for the forward and reverse reactions). For nNOS CaM$^+$, transients obtained under pseudo-first-order conditions (10-fold excess NADPH), at 458 nm over a 500 ms time period from the mixing event, were best fit to a triphasic exponential expression [eqn (1); Figure 3A], consistent with the three phases identified in photodiode array experiments over the same timescale; fitting to mono- or bi-phasic exponential expressions produced systematic deviations indicating poor fitting to the data. The slowest phase observed in the photodiode array experiments over a 10 s period (species D $\rightarrow$ E) is not observed on the shorter time period of 500 ms in single-wavelength mode. Single-wavelength transients were collected using a 'split' time-base utility in the acquisition software of the stopped-flow instrument, to maximize the number of data points in the early phase of the transient. For nNOS CaM$^+$, the rate constants for each of the three phases are 580 s^{-1}, 27 s^{-1} and 5 s^{-1}. Similar transients were observed with nNOS CaM$^-$ (Figure 3D); in this case the rate constants for the three phases are 545 s^{-1}, 43 s^{-1} and 6.6 s^{-1}. The proteolysed form of nNOS reductase also behaved similarly to nNOS CaM$^+$ and nNOS CaM$^-$ (455 s^{-1}, 38 s^{-1} and 8 s^{-1}; transients not shown). Extension of the time base to 10 s from mixing enabled access to the fourth slow phase, although the fast first phase (A $\rightarrow$ B) is almost completely lost (Figures 3C and 3F). Fitting over this time period was therefore also achieved using a triphasic exponential function (species B $\rightarrow$ C $\rightarrow$ D $\rightarrow$ E) and yielded rate constants for the conversion of D $\rightarrow$ E of 0.3 s^{-1} (nNOS CaM$^+$) and 0.3 s^{-1} (nNOS CaM$^-$). The four rate constants obtained from single-wavelength absorption studies at 458 nm for each of the nNOS reductase domains are consistent with the spectral changes observed by photodiode array detection (Figures 1 and 2). The only relatively minor discrepancy is the $\approx$ 2-fold difference in the observed rate constant for the conversion of A $\rightarrow$ B calculated from data collected in single-wavelength mode and photodiode array detection. However, the conversion of A $\rightarrow$ B is relatively fast, and difficult to analyse, using the stopped-flow method with an instrument dead-time of 1 ms. Also, in photodiode array detection, the first spectrum is collected at 1.28 ms (instrument dead-time is 1 ms), and thus more of the fast phase is lost than in single-wavelength mode. This may account for the smaller rate constants determined by global fitting of photodiode array data. Given the limitations of the stopped-flow method in analysing the fast phase and the complexity of the fitting process, the values of $\approx$ 500 s^{-1} for this phase should be regarded as being approximate.

To aid in the assignment of kinetic phases, stopped-flow experiments, in which the fluorescence emission of NADPH at 450 nm was monitored following excitation at 340 nm, were performed. For nNOS CaM$^+$, over a short time period (500 ms), fluorescence transients were biphasic (rate constants 63 s^{-1} and 6.5 s^{-1}; Figure 3B), but over a 10 s time base, triphasic transients were observed, owing to the appearance of an additional slow phase (rate constant 0.4 s^{-1}; Figure 3B, inset). The rate constants for the three kinetic phases seen over 10 s are similar to those observed for three of the phases observed in absorption studies, corresponding to the conversion of spectral species B $\rightarrow$ C $\rightarrow$ D $\rightarrow$ E. As discussed later, the slow phase (D $\rightarrow$ E) is not relevant in steady-state turnover and likely reflects further oxidation of NADPH as a result of thermodynamic relaxation of reduced nNOS reductase via a series of disproportionation reactions (also seen with CPR [25]) and/or conformational change. The fluorescence data indicate that NADPH is oxidized during the conversion of spectral species B $\rightarrow$ C and C $\rightarrow$ D. Significant fluorescence changes were not observed on a time scale consistent with the conversion of A $\rightarrow$ B (i.e. establishment of the equilibrium between the NADPH-enzyme charge-transfer species and two electron reduced NOS complexed with NADP$^+$). However, the absorbance transients at 458 nm (Figures 3A and 3D) indicate that the flavin absorbance is bleached during the fast kinetic phase (A $\rightarrow$ B), consistent with there being some reduction of the enzyme by NADPH. That C-H bond breakage occurs during the conversion of species A into species B is demonstrated by the kinetic isotope effect (KIE $\approx$ 2) seen with A-side NADP^{2}H in absorption transients at 450 nm (Figure 4A). With NADP^{2}H, the amplitude of the fast phase (A $\rightarrow$ B) is increased substantially as less signal is lost in the dead-time of the stopped-flow instrument. Significant kinetic isotope effects are not seen in the conversion of B $\rightarrow$ C and C $\rightarrow$ D in both absorption and fluorescence measurements (Figures 4A and 4B), although substantial flavin reduction and NADP^{2}H oxidation accompanies these reactions. We therefore infer that a process, other than C-H(^{2}H) bond breakage, limits the rate of conversion of B $\rightarrow$ C and C $\rightarrow$ D, and suggest that further reduction of flavin in these steps is gated by the release of NADP$^+$. These assignments are consistent with a reversible kinetic scheme of the type shown (Scheme 1).

A puzzling aspect of our kinetic data is the lack of significant fluorescence change accompanying NADPH oxidation in the fast kinetic step (A $\rightarrow$ B), which represents the rapid establishment of the equilibrium between the enzyme-NADPH charge-transfer species, and the two-electron-reduced enzyme complexed with NADP$^+$. Similar observations were made in our studies with human CPR [25], in which an equivalent equilibrium is established rapidly on mixing enzyme with NADPH. Likewise we have shown the lack of a fluorescence change in stopped-flow studies with the CPR analogue NR1, even though absorption studies indicate that the flavin is almost fully reduced. We have no mechanistic explanation for the lack of appreciable fluorescence in these reactions, but that C-H bond breakage occurs on conversion of spectral species A $\rightarrow$ B is indicated in our studies with A-side NADP^{2}H and the bleaching of flavin absorption at 458 nm.

The reversibility of flavin reduction is apparent from sequential stopped-flow studies of enzyme oxidation (Figures 5A and 5B). In these experiments, nNOS CaM$^+$ was mixed with a 2-fold excess of NADPH to effect reduction of the flavins. After a suitable aging time (1 s), a 20-fold excess of NADP$^+$ was mixed with the sample. Absorption changes at 458 nm indicate oxidation of the flavins on mixing with NADP$^+$, and fluorescence changes indicate that NADPH formation accompanies flavin oxidation. At longer time excursions, there is a small reduction in the absorbance at 458 nm and fluorescence at 450 nm as the system relaxes to its most thermodynamic stable state.

Our stopped-flow studies indicate that the kinetics of flavin reduction are similar for nNOS CaM$^+$ (Figures 1 and 3), nNOS CaM$^-$ (Figures 2 and 3) and the proteolysed form of nNOS (Figure 2). CaM binding does not affect the kinetics of conversion of B $\rightarrow$ C and C $\rightarrow$ D [16], suggesting that NADP$^+$ release is not triggered by CaM binding. As discussed above, determination of accurate rate constants for the conversion of species A $\rightarrow$ B is difficult in stopped-flow studies at 458 nm (fitted rate constants $\approx$ 500 s^{-1}), owing to the complex nature of the transients and the rapid conversion of A $\rightarrow$ B. Consequently, it is difficult to demonstrate unequivocally any effect of CaM binding on the kinetics of conversion of A $\rightarrow$ B from single-wavelength data collected at 458 nm.

We have also performed stopped-flow absorption studies at 600 nm to investigate in more detail the small absorption changes at this wavelength. The photodiode array experiments (Figures 1 and 2) suggest that there is little absorption change in this region, but the inherent noise associated with photodiode array acquisition

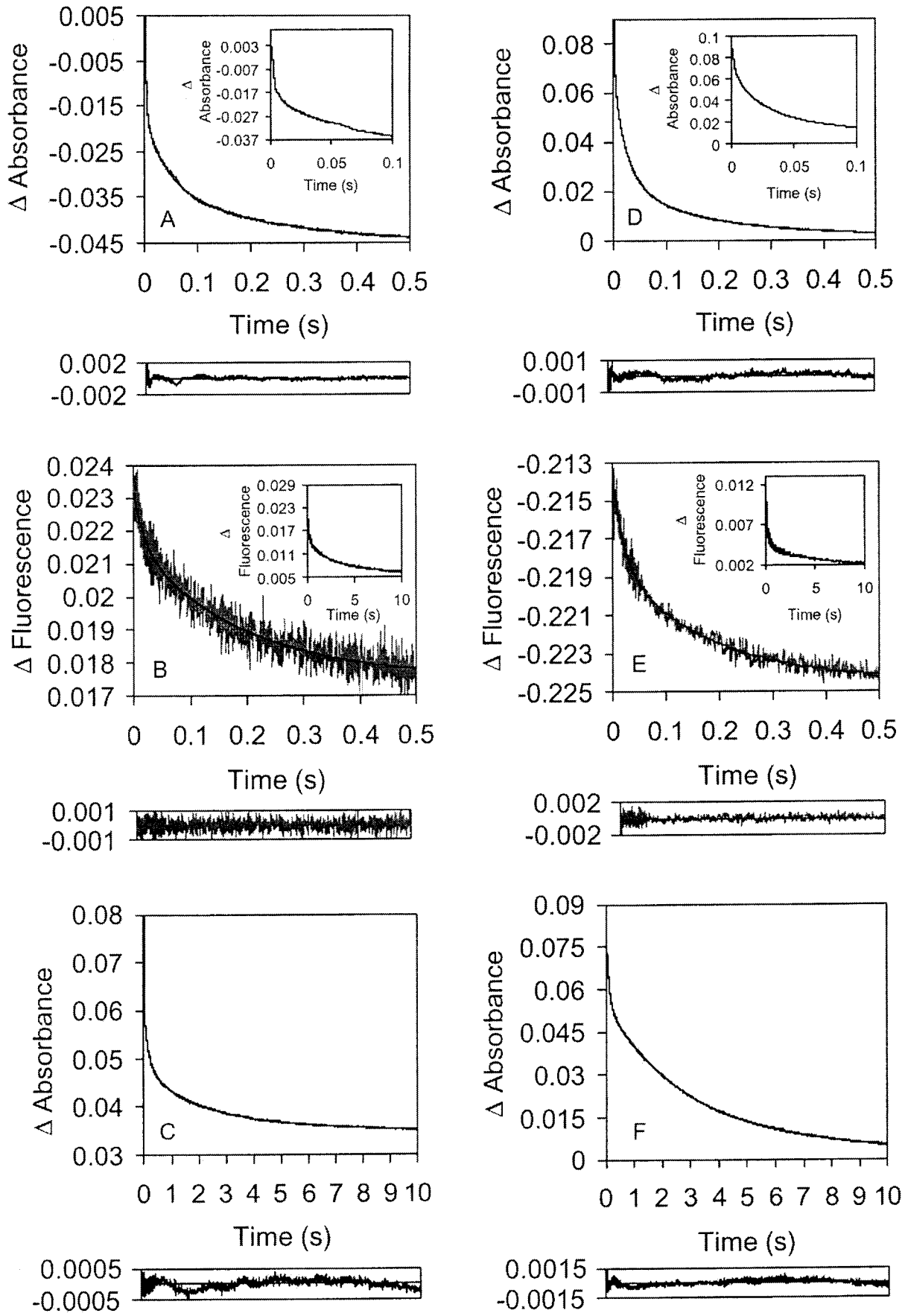

Figure 3 For caption see facing page.

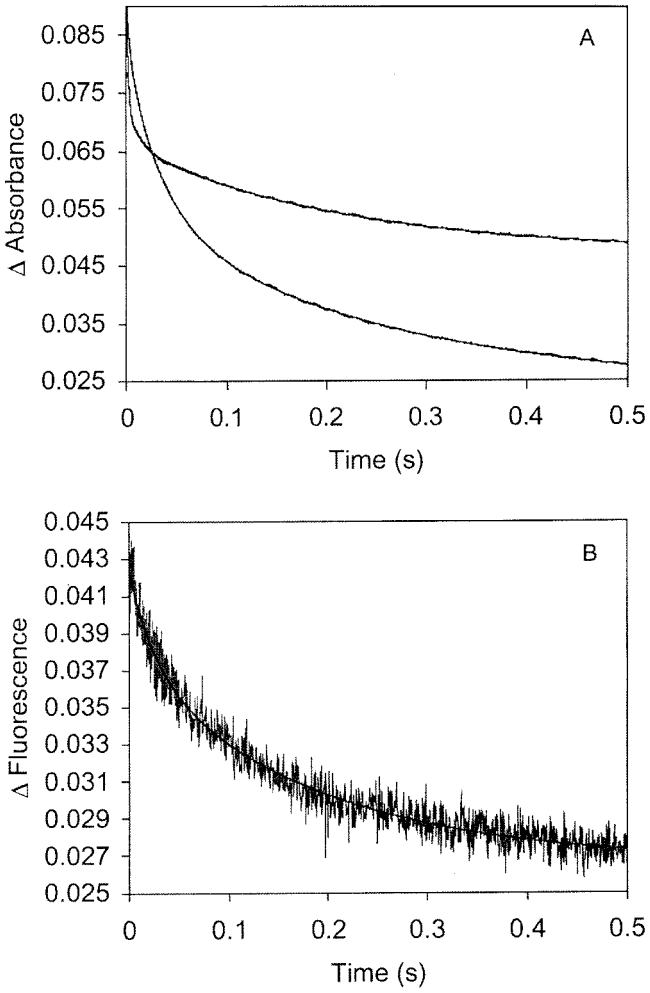

Figure 4 Absorption and fluorescence transients for the reduction of nNOS CaM$^+$ with NADPH and NADP^{2}H

(**A**) Absorption transient at 458 nm. Upper transient is for NADPH; lower transient is for NADP^{2}H. Rate constants for the three phases observed with NADP^{2}H were determined by fitting to eqn (1) and are 214, 28 and 3.7 s^{-1}, respectively. (**B**) Fluorescence transient recorded at 450 nm for the reaction of nNOS CaM$^+$ with NADP^{2}H. Fitting to a biphasic expression yields rate constants of 37 and 5.3 s^{-1}.

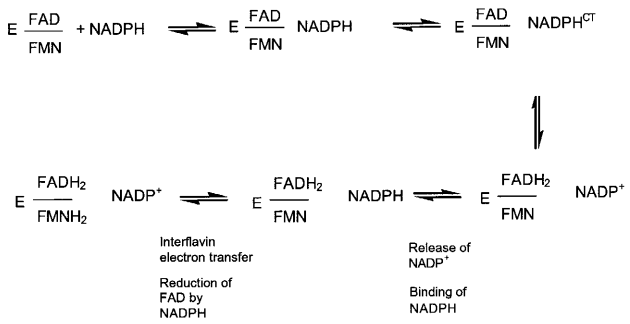

Scheme 1 Reductive half reaction of nNOS reductase domain

The scheme indicates the major enzyme species that form in stopped-flow studies of the reduction of nNOS reductase by NADPH. See text for detailed discussion.

does not allow investigation of the very small absorption changes using this method of detection. To improve the signal-to-noise, single-wavelength experiments were performed at 600 nm with nNOS CaM$^+$ and nNOS CaM$^-$ using a 25-fold excess of NADPH (Figures 6A and 6B respectively). The transients obtained for both forms of the enzyme are qualitatively similar. Over a short time period (500 ms) the absorption at 600 nm climbs very rapidly ($k \approx 500\ s^{-1}$). The signal then declines ($k \approx 40\ s^{-1}$) and then climbs again over an extended time period (10 s). Repeated measurement of this slow increase in absorption suggests it is biphasic with rate constants $\approx 10\ s^{-1}$ and $\approx 0.4\ s^{-1}$ (precise values are difficult to obtain owing to the small signal change). Again, these four kinetic phases can be correlated with the scheme proposed from our photodiode array experiments. The very fast increase in absorption ($k \approx 500\ s^{-1}$) indicates the formation of an enzyme-NADPH charge-transfer intermediate, and is consistent with the rapid establishment of an equilibrium between an NADPH-enzyme charge-transfer species and two-electron-reduced enzyme bound to NADP$^+$ (i.e. A $\rightarrow$ B). This increase in absorption is slightly faster for nNOS CaM$^+$, as indicated by the elevated absorption immediately after mixing compared with the comparable transient for nNOS CaM$^-$, suggesting that CaM binding accelerates, albeit modestly, the establishment of the equilibrium between the NADPH-enzyme charge-transfer species and two-electron-reduced enzyme bound to NADP$^+$. This increase in absorption at 600 nm is relatively small and it should not be confused with the formation of a blue di-semiquinonoid intermediate. The second phase ($\approx 40\ s^{-1}$) is consistent with further reduction of the flavin following release of NADP$^+$, leading to loss of the charge-transfer signature at 600 nm (i.e. the equilibrium between the NADPH-enzyme charge-transfer species and two-electron-reduced enzyme bound to NADP$^+$ is displaced further towards flavin reduction by loss of NADP$^+$). We postulate that NADP$^+$-release from two-electron-reduced NOS is relatively slow and thus gates internal electron transfer (hence the absence of signature for the blue di-

Figure 3 Single wavelength absorption and fluorescence transients for the reactions of nNOS CaM$^+$ and nNOS CaM$^-$ with NADPH

Conditions as for Figure 1. [Enzyme] = 5 μM; [NADPH] = 50 μM. (**A**) Absorption transient at 458 nm for reduction of nNOS CaM$^+$. Transient is fitted using eqn (1) (rate constants 580, 27, 5 s^{-1}). Inset, the early time domain of the transient shown in the main panel. (**B**) NADPH fluorescence transient for nNOS CaM$^+$. Transient fitted to a standard biphasic expression (rate constants 63 and, 6.5 s^{-1}). Inset, NADPH fluorescence transient over a longer time period (10 s) to illustrate the presence of the third slow phase (0.4 s^{-1}) also observed in absorption experiments (**C**). (**C**) Absorption change at 458 nm over a 10 s period for nNOS CaM$^+$. Approximate fitting to a triphasic expression yielded a rate constant of 0.3 s^{-1} for the slow phase. (**D**) as for (**A**), except panel shows reduction of nNOS CaM$^-$ (rate constants 545, 43, 6.6 s^{-1}). (**E**) as for (**B**), except panel shows NADPH fluorescence transient for nNOS CaM$^-$ (rate constants 52 and 5.9 s^{-1}). Inset, NADPH fluorescence transient over a longer time period (10 s) to illustrate the presence of the third slow phase (0.25 s^{-1}), which was also observed in absorption experiments (**F**). (**F**), as for (**C**) except panel shows absorbance change for nNOS CaM$^-$. For (**C**) and (**F**), the rate constants for the 'faster phase' of these transients (B $\rightarrow$ C) is contaminated by the fast conversion of A $\rightarrow$ B seen over shorter time periods. Consequently, the values of the rate constant for the conversion of B $\rightarrow$ C is overestimated in this fitting process. If the fit range is truncated such that the very early part of the transient is omitted, the fast phase approaches a value of $\approx 40\ s^{-1}$, which is expected from both fluorescence and absorption data over shorter time periods. Fitting of fluorescence data for the proteolysed nNOS reductase gave rate constants of 40, 3.6 and 0.3 s^{-1} (transient not shown); comparable absorption data gave rate constants of 455, 38 and 8 s^{-1} (results not shown).

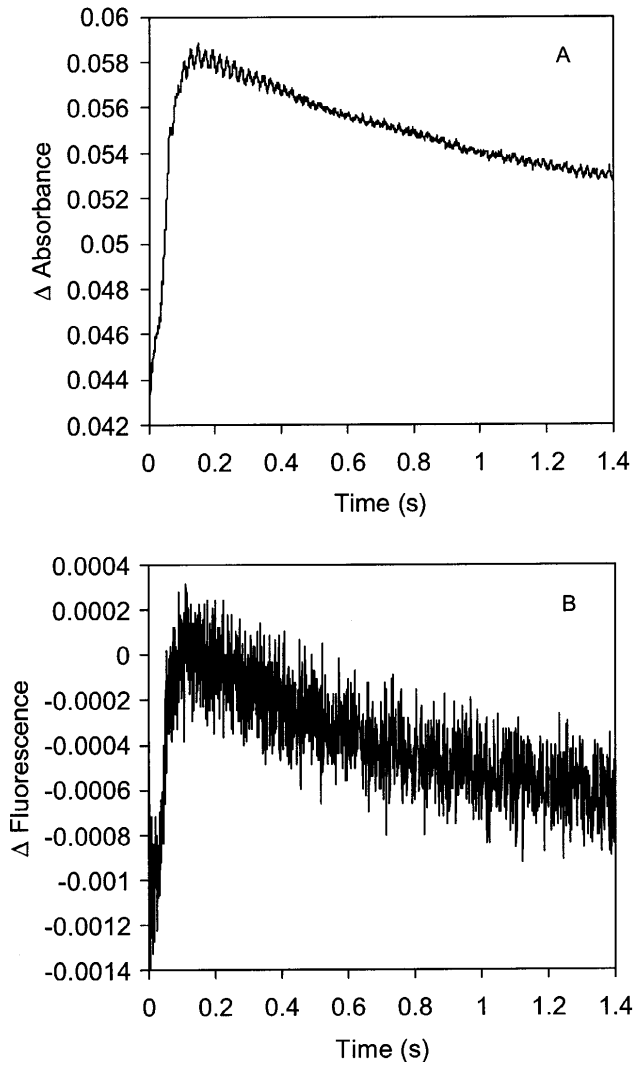

Figure 5 Absorption and fluorescence transients illustrating reverse electron transfer in nNOS CaM$^+$

Enzyme was pre-reduced with NADPH in the first mix followed by rapid mixing with NADP$^+$. Conditions: [nNOS CaM$^+$] = 5 μM; [NADPH] = 10 μM; [NADP$^+$] = 100 μM; aging time = 1 s. (**A**) Absorption transient observed at 458 nm. (**B**) Fluorescence transient observed at 450 nm.

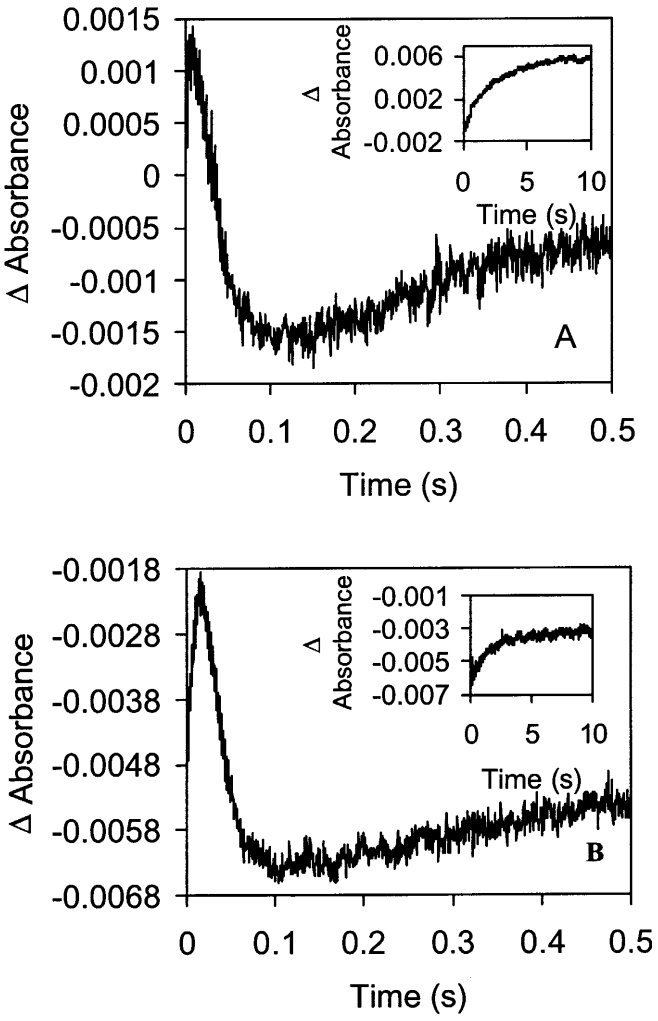

Figure 6 Absorption transients for the reduction of nNOS CaM$^+$ and nNOS CaM$^+$ at long wavelength

Conditions: as for Figure 3. (**A**) Absorption change of nNOS CaM$^+$ at 600 nm over a 500 ms time period. Inset: transient recorded over an extended time period (10 s). (**B**) Absorption change of nNOS CaM$^-$ at 600 nm over a 500 ms time period. Inset: transient recorded over an extended time period (10 s). Approximate rate constants were determined by fitting to eqn (2) and are given in the text. Fitting was performed for the time period 0 to 0.1 s.

semiquinoid form of nNOS reductase following hydride transfer). Binding of the second NADPH and subsequent hydride transfer occurs in the third kinetic phase; the fourth kinetic phase ($\approx 0.4\ s^{-1}$) is not catalytically important, and as discussed below may reflect conformational realignment and/or disproportionation (as seen in CPR) of nNOS reductase following reduction by NADPH. A rationale for the increase in absorption at 600 nm which accompanies the third kinetic phase is less clear. A number of possibilities exist, depending on the equilibrium distribution of enzyme species. These include (i) incomplete reduction of nNOS to the four-electron level, thus leaving a small proportion of two-electron-reduced enzyme, which after NADP$^+$ release would be in the blue di-semiquinoid form (incomplete reduction is consistent with the known potentials of the flavin couples); (ii) slow conformational change and (iii) slow development of a reduced enzyme species complexed with NADPH. Clearly, the mechanistic basis for these small increases in absorption at long time base is complex and beyond the scope of the present paper.

Concentration-dependence of flavin reduction and charge-transfer formation

Having established the sequence of events in the kinetic model proposed from our photodiode array analysis of the reduction of nNOS reductase domain by NADPH (Scheme 1), we sought additional evidence for our kinetic model by studying the concentration-dependence of the kinetic phases. For both

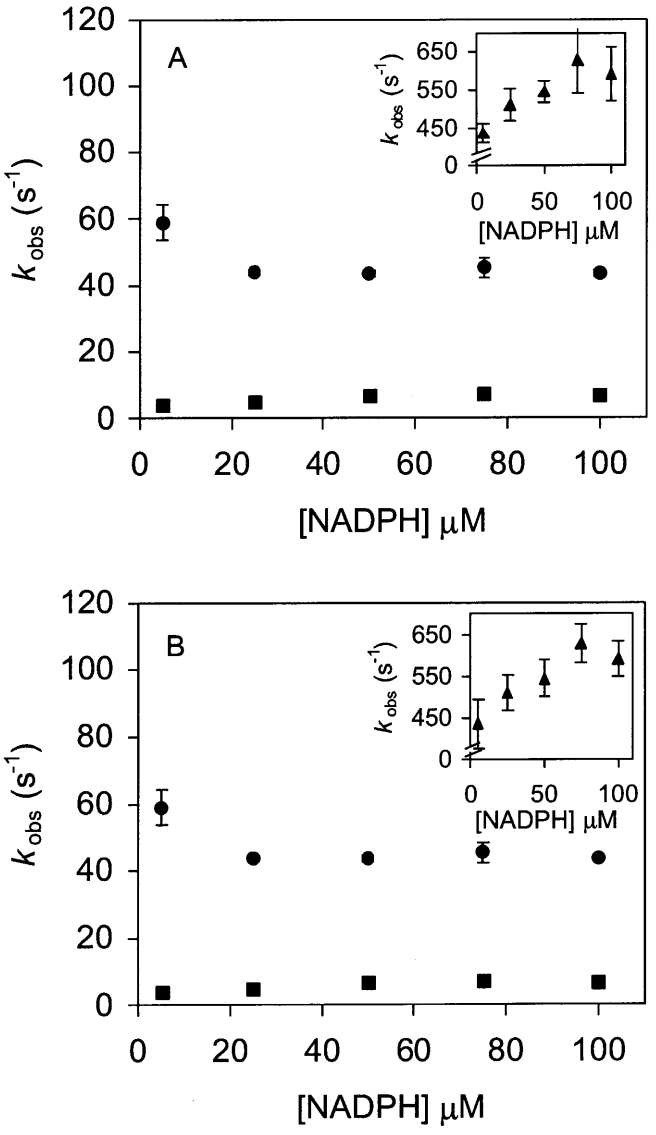

Figure 7 Plots illustrating the variation in observed rate constants for selected kinetic phases as a function of NADPH concentration for nNOS CaM$^+$ and nNOS CaM$^-$

(**A**) Data for nNOS CaM$^+$; filled circles, observed rate for conversion of B → C; filled squares, observed rate for conversion of C → D. Inset, observed rate for conversion of A → B. (**B**) Data for nNOS CaM$^-$; symbol definitions as for panel A. Error bars represent one standard deviation calculated from the average of five reductive transients.

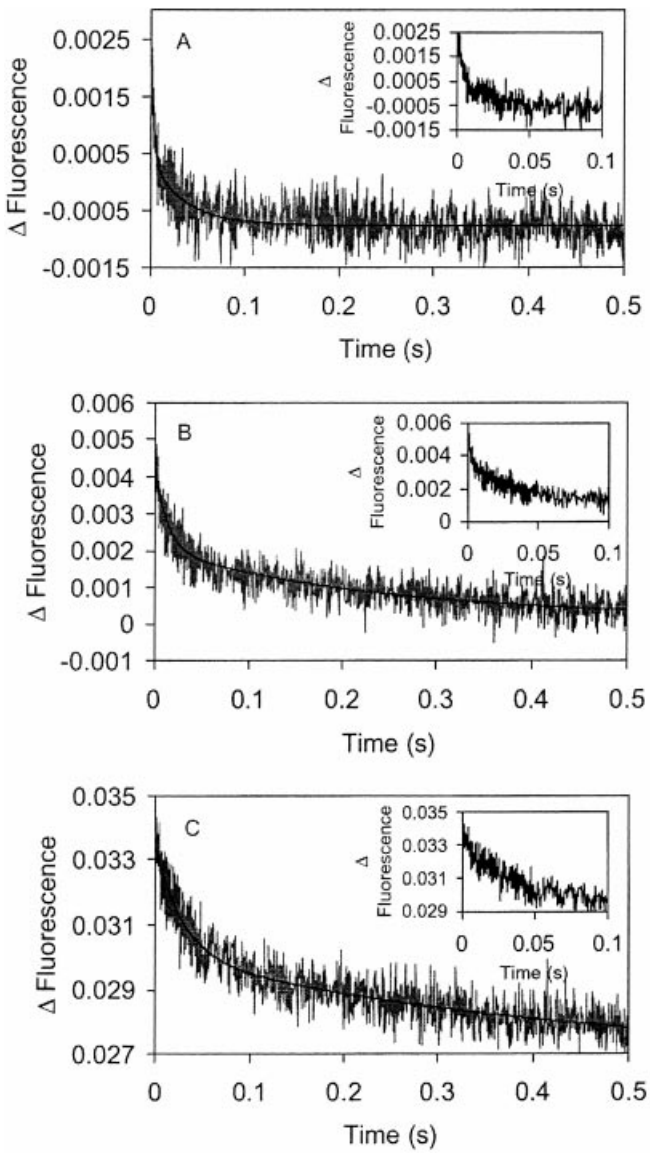

Figure 8 Fluorescence transients for the reduction of nNOS CaM$^+$ by NADPH

[Enzyme] = 5 μM. (**A**) Reaction with 5 μM NADPH. (**B**) Reaction with 10 μM NADPH. (**C**) Reaction with 50 μM NADPH. The data clearly indicate that the rate of NADPH oxidation increases as the NADPH concentration approaches stoichiometric levels. Insets; expansion of the early part of the transients shown in panels A to C.

the nNOS CaM$^+$ and nNOS CaM$^-$ enzymes, the observed rate constants for the conversion of spectral species B → C and C → D are independent of NADPH concentration in the pseudo-first-order regime (Figure 7). This finding is consistent with similar studies that we have performed on human CPR [25]. Also, we have demonstrated with nNOS reductase an increase in the observed rate constant for conversion of B → C at low NADPH concentration (i.e. at NADPH concentrations < 5-fold the enzyme concentration; Figures 7 and 8). These findings are also consistent with our work on human CPR that enabled us to propose the existence of a second NADPH-binding site [25]. Binding of a second molecule of NADPH to the two-electron-reduced-enzyme bound to NADP$^+$ should sterically hinder the release of NADP$^+$ from the reduced enzyme. Since further reduction of the flavin is rate-limited by NADP$^+$ release (B → C), this would account for the slower rates of flavin reduction (and NADPH oxidation) at relatively high coenzyme concentrations. Nicotinamide coenzymes bind to CPR in a bipartite fashion; electron density for the ribose-nicotinamide portion is poorly defined in the structure of rat CPR, whereas the 2′P-AMP portion is clear [9]. This bipartite recognition in CPR might account for the attenuation of flavin reduction rate at high nicotinamide coenzyme concentrations. In one model for regulation of flavin reduction rate, the reducing coenzyme interacts predominantly with the 2′P-AMP pocket. This interaction would

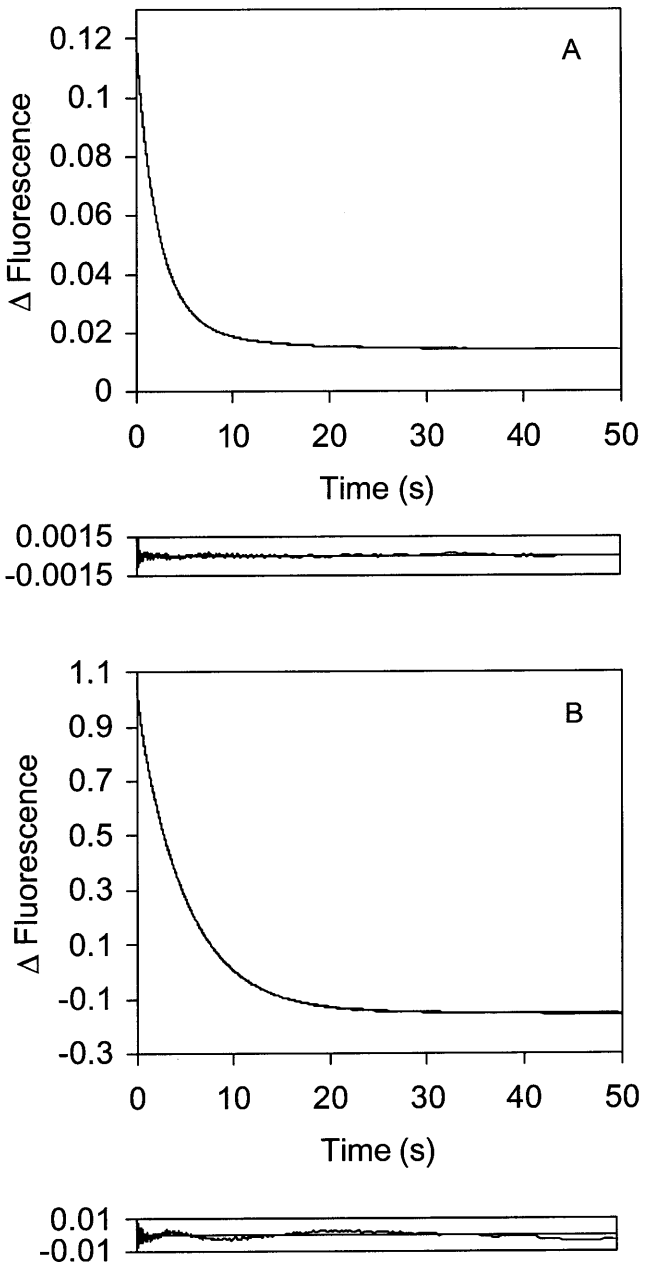

Figure 9 Transients for change in flavin fluorescence on reaction of nNOS CaM$^+$ and nNOS CaM$^-$ with NADPH

Conditions as for Figure 3. Fluorescence emission measured at 530 nm; excitation at 450 nm. (**A**) Transient for nNOS CaM$^+$. (**B**) Transient for nNOS CaM$^-$.

likely impede NADP$^+$-release bound predominantly in the NMN-binding pocket. Thus, the binding of two coenzyme molecules to the same bipartite coenzyme-binding site may be responsible for the lower rates of flavin reduction within CPR and also in nNOS reductase at high NADPH concentrations. A complete understanding of the regulatory mechanism for flavin reduction, however, must await further structural studies of coenzyme complexes of nNOS reductase.

Within the constraints of the stopped-flow method, we also investigated the concentration-dependence of the fast phase (A → B) at 458 nm, which reports on the establishment of the initial equilibrium between the NADPH-enzyme charge-transfer species and the two-electron-reduced-enzyme bound to NADP$^+$. Our data suggest that these observed rate constants for conversion of A → B are independent of coenzyme concentration, although as discussed above, the errors in the determined rate constants are appreciable. Our findings suggest that species A in our kinetic scheme is an oxidized enzyme species, bound to coenzyme, but with the NMN portion sub-optimally positioned over the flavin, thus preventing the development of the charge-transfer complex and flavin reduction.

Flavin fluorescence emission in single-turnover studies

We have also conducted stopped-flow studies in which the fluorescence emission of the flavins in nNOS CaM$^+$ and nNOS CaM$^-$ was measured during enzyme reduction (Figure 9). Kinetic transients for nNOS CaM$^+$ and nNOS CaM$^-$ were found to be similar. However, unlike the transients for NADPH emission, and the flavin absorption transients, the flavin fluorescence changes occur predominantly on an extended time scale. Fitting to these transients was approximated using a tri-exponential expression, with the major reduction in emission of flavin fluorescence occurring in the second phase. For nNOS CaM$^+$, the fast phase (1.4 s^{-1}) is associated with a small amplitude (5 % of the total amplitude change); the second phase (0.23 s^{-1}) accounts for $\sim$ 80 % of the total fluorescence change, and the third phase (0.16 s^{-1}) accounts for $\approx$ 15 % of the total fluorescence change. Similar values are observed for nNOS CaM$^-$. Clearly, these fluorescence changes occur on time scales much slower than the redox processes identified in the NADPH fluorescence and flavin absorption studies, and consequently they likely report on conformational changes in the vicinity of the flavin cofactors that occur as a result of flavin reduction and/or disproportionation. In this regard, it is important to note that Brunner and coworkers [35] have demonstrated that the fluorescence intensity of the two flavin groups in nNOS decays highly nonexponentially and they suggest this excited-state heterogeneity is the result of multiple flavin-quenching sites arising from altered flavin microenvironments. Although we have fitted our data to a tri-exponential process, we cannot exclude the occurrence of more complex conformational processes with overlapping time constants. Our data indicate that the major flavin fluorescence changes occur on time scales that are not catalytically important, and that they are most likely linked to conformational events.

DISCUSSION

A detailed understanding of the mechanism of electron transfer in the reductase domain of NOS is key to our appreciation of the varied effects of ligand binding and the mechanism of substrate reduction. Previous studies have established that CaM binding facilitates electron transfer from the flavoprotein reductase domain to the oxygenase domain of NOS [15], giving rise to a stimulation of NO synthesis in the presence of calcium and CaM. Superoxide generation by the oxygenase domain is also CaM-dependent, but production of superoxide by the reductase domain is independent of CaM [36], despite reports that CaM binding enhances flavin reduction in nNOS reductase [16]. In full length NOS, CaM binding increases cytochrome *c* reductase and ferricyanide activities by 11.5- and 1.7-fold respectively, and stimulation (8.9- and 1.9-fold respectively) is still observed in NOS that has been depleted of haem and BH_4 [16]. Similar enhancement (11.6- and 3.7-fold respectively) by CaM of basal

cytochrome *c* and ferricyanide reduction activity is also observed with the isolated nNOS reductase domain [31], which is in contrast to the lack of stimulation seen for superoxide production [36]. Given the complexity of the responses to CaM binding in NOS, and in particular the reductase domain, in this paper we undertook a detailed study of the electron-transfer mechanism in the reductase domain. By performing studies in the presence and absence of CaM we have attempted to resolve some of the complex issues raised above.

In our stopped-flow studies we elected to concentrate on the isolated reductase domain rather than full-length nNOS, owing to the reduced number of chromophores in the reductase domain. This type of 'reductionist' approach has been useful in our studies of human CPR, in which studies of individual domains allowed us to identify new intermediates not observed readily in the full-length enzyme [25]. Our stopped-flow studies with nNOS reductase have revealed the complex nature of the reductive half-reaction. In previous work, the absorption changes at 458 nm were approximated to biphasic processes [24]. Although our absorbance transients are similar to those published by others, we have demonstrated that these transients are substantially 'contaminated' by additional spectral signals arising from the formation of additional intermediates. Moreover, our photodiode array data indicates the lack of a blue di-semiquinonoid intermediate during enzyme reduction, requiring reappraisal of previously published kinetic mechanisms for nNOS reductase, which have invoked the presence of this intermediate [18]. We have identified at least three kinetic phases involving flavin reduction and oxidation of NADPH. The first reductive step (A → B) represents the rapid formation of an equilibrium between an NADPH-enzyme charge-transfer species and two-electron-reduced-enzyme bound to $NADP^+$. The second and third steps represent further reduction of the enzyme flavins limited by the rate of $NADP^+$ release. A fourth slow phase is not relevant to catalysis and probably represents conformational change and/or disproportionation. The observed rate constants for conversion of spectral species B → C and C → D ($\approx 50\ s^{-1}$ and $5\ s^{-1}$) which reflect $NADP^+$ release from reduced enzyme, and spectral species A → B (establishment of the equilibrium between E–NADPH and $NADP^+$–reduced enzyme) are in-line with those reported for comparable studies with human CPR. The rate constant for conversion of B → C is similar to that reported for haem reduction ($49\ s^{-1}$) and ferrous nitrosyl complex formation ($36\ s^{-1}$) for full-length nNOS [24]. The true k_{cat} measured for nNOS under steady-state conditions with cytochrome *c* as electron acceptor is $37\ s^{-1}$ [37]. The kinetic steps C → D and D → E are therefore clearly not relevant in steady-state turnover, although one needs to bear in mind that the redox states of NOS populated under steady-state conditions are not yet clearly defined.

We have shown that the blue di-semiquinoid species (FAD_{sq}, FMN_{sq}) do not accumulate in stopped-flow studies of nNOS reductase, suggesting that internal electron transfer between the flavins is relatively slow and gated by $NADP^+$ release. A reason for this disparity in the behaviour of nNOS reductase and CPR may be found in the nature of the residue positioned close to the *re* face of the isoalloxazine ring of the FAD. In human CPR this residue (Trp^{676}) facilitates the release of $NADP^+$ following the first hydride transfer; mutation to histidine (Trp^{676} → His CPR) impairs $NADP^+$ release (and internal electron transfer to FMN) by stabilizing a reduced enzyme-$NADP^+$ charge-transfer intermediate [26]. The corresponding residue in rat nNOS is Phe^{1395} [38] and is presumed to play an analogous role in the mechanism of release of $NADP^+$. However, this release step is impaired in nNOS, thus preventing rapid internal electron transfer to FMN. Recent kinetic isotope effect studies with nNOS reductase indicate that the reductive half-reaction is more rate-limiting than the oxidative half-reaction in reactions with cytochrome *c* [39]. The slow step in the reductive half-reaction is not associated with hydride transfer and may reflect the release of nicotinamide coenzyme from the reductase domain. This is consistent with the notion that coenzyme exchange facilitated by Phe^{1395} is less effective than in human CPR where mutation of Trp^{676} is known to impair displacement of the nicotinamide coenzyme from the active site [26].

The lack of a major effect attributed to CaM binding on the rate constants for flavin reduction and charge-transfer complex formation (A → B), and the absence of any effect on the kinetics of further reduction of the flavin (B → C and C → D), are in stark contrast with previous reports on the mechanism of flavin reduction in nNOS reductase [16]. These latter studies have relied solely on absorption measurements to study the rate of flavin reduction, and data were fitted to a single-exponential function, which is clearly inappropriate given the complexity of the reactions discussed herein. Our stopped-flow studies also rule out any effect of CaM binding on interflavin electron transfer, and bring into question previous reports that claim enhanced rates of internal electron transfer for nNOS reductase in the presence of CaM [17]. Additional studies are clearly required to account for the stimulation of cytochrome *c* reduction by CaM and it seems likely that CaM-stimulation of basal cytochrome *c* reductase activity in steady-state assays is associated with the electron transfer step between reductase and cytochrome *c*. Cytochrome *c* is an artificial redox acceptor and likely interacts at a number of sites on the surface of nNOS reductase. It is conceivable, therefore, that CaM influences this interaction. Stopped-flow analysis of cytochrome *c* reduction by nNOS reductase is not straightforward since the reduction of nNOS reductase with NADPH or dithionite (by titration to the two-electron level) prior to mixing would generate the blue semiquinone form. Since this species is not observed in stopped-flow turnover studies, its relevance to steady-state turnover needs to be addressed. Our current work is now focused on developing sequential mixing protocols to transiently generate reduced nNOS reductase that are suitable for stopped-flow studies with cytochrome *c*.

Concluding remarks

The kinetic mechanism of nNOS reductase has been re-evaluated in the light of new stopped-flow data. Our absorption transients for flavin reduction at 458 nm and 600 nm are similar to those published previously, but our fluorescence and photodiode array data indicate inappropriate fitting in earlier work, leading to incorrect assignment of kinetic phases and mis-identification of enzyme intermediates. We show that a charge-transfer complex accumulates prior to flavin reduction, and that flavin reduction is relatively slow. We have also shown that the air-stable blue semiquinone does not accumulate under stopped-flow conditions. Contrary to dogma, CaM does not significantly enhance the rate of flavin reduction in nNOS reductase. Internal electron transfer between the flavins is relatively slow, and probably gated by $NADP^+$ release. The study highlights the danger of only using single-wavelength absorption transients to measure the rates of individual chemical steps in a complex series of reactions and emphasizes the need to perform complementary multiple-wavelength absorption and fluorescence experiments in studies of complex flavoenzymes.

This work was funded by the U.K. Biotechnology and Biological Sciences Research Council (studentship to K.K.), the Wellcome Trust and the Lister Institute of Preventive Medicine. N.S.S. is a Lister Institute Research Professor.

REFERENCES

1 Ignarro, L. J., Buga, G. M., Wood, K. S., Byrns, R. E. and Chaudhuri, G. (1987) Endothelium-derived relaxing factor produced and released from artery and vein is nitric oxide. Proc. Natl. Acad. Sci. U.S.A. **84**, 9265–9269

2 Palmer, R. M., Ferrige, A. G. and Moncada, S. (1987) Nitric oxide release accounts for the biological activity of endothelium-derived relaxing factor. Nature (London) **327**, 524–526

3 Garthwaite, J., Charles, S. L. and Chess-Williams, R. (1988) Endothelium-derived relaxing factor release on activation of NMDA receptors suggests role as intercellular messenger in the brain. Nature (London) **336**, 385–388

4 Griffith, O. W. and Stuehr, D. J. (1995) Nitric oxide synthases: properties and catalytic mechanism. Annu. Rev. Physiol. **57**, 707–736

5 Stuehr, D. J. (1997) Structure-function aspects in the nitric oxide synthases. Annu. Rev. Pharmacol. Toxicol. **37**, 339–359

6 Marletta, M. A. (1993) Nitric-oxide synthase structure and mechanism. J. Biol. Chem. **268**, 12231–12234

7 Bredt, D. S. and Snyder, S. H. (1994) Nitric oxide: a physiologic messenger molecule. Annu. Rev. Biochem. **63**, 175–195

8 Bredt, D. S., Hwang, P. M., Glatt, C. E., Lowenstein, C., Reed, R. R. and Snyder, S. H. (1991) Cloned and expressed nitric oxide synthase structurally resembles cytochrome P-450 reductase. Nature (London) **351**, 714–718

9 Wang, M., Roberts, D. L., Paschke, R., Shea, T. M., Masters, B. S. and Kim, J. J. (1997) Three-dimensional structure of NADPH-cytochrome P450 reductase: prototype for FMN- and FAD-containing enzymes. Proc. Natl. Acad. Sci. U.S.A. **94**, 8411–8416

10 Leclerc, D., Wilson, A., Dumas, R., Gafuik, C., Song, D., Watkins, D., Heng, H. H., Rommens, J. M., Scherer, S. W., Rosenblatt, D. S. and Gravel, R. A. (1998) Cloning and mapping of a cDNA for methionine synthase reductase, a flavoprotein defective in patients with homocystinuria. Proc. Natl. Acad. Sci. U.S.A. **95**, 3059–3064

11 Paine, M. J., Garner, A. P., Powell, D., Sibbald, J., Sales, M., Pratt, N., Smith, T., Tew, D. G. and Wolf, C. R. (2000) Cloning and characterization of a novel human dual flavin reductase. J. Biol. Chem. **275**, 1471–1478

12 McMillan, K. and Masters, B. S. S. (1995) Prokaryotic expression of the heme-binding and flavin-binding domains of rat neuronal nitric-oxide synthase as distinct polypeptides – identification of the heme-binding proximal thiolate ligand as cysteine-415. Biochemistry **34**, 3686–3693

13 Cho, H. J., Xie, Q. W., Calaycay, J., Mumford, R. A., Swiderek, K. M., Lee, T. D. and Nathan, C. (1992) Calmodulin is a subunit of nitric oxide synthase from macrophages. J. Exp. Med. **176**, 599–604

14 Sheta, E. A., McMillan, K. and Masters, B. S. S. (1994) Evidence for a bidomain structure of constitutive cerebellar nitric oxide synthase. J. Biol. Chem. **269**, 15147–15153

15 Abu-Soud, H. M. and Stuehr, D. J. (1993) Nitric oxide synthases reveal a role for calmodulin in controlling electron transfer. Proc. Natl. Acad. Sci. U.S.A. **90**, 10769–10772

16 Abu-Soud, H. M., Yoho, L. L. and Stuehr, D. J. (1994) Calmodulin controls neuronal nitric-oxide synthase by a dual mechanism. Activation of intra- and interdomain electron transfer. J. Biol. Chem. **269**, 32047–32050

17 Matsuda, H. and Iyanagi, T. (1999) Calmodulin activates intramolecular electron transfer between the two flavins of neuronal nitric oxide synthase flavin domain. Biochim. Biophys. Acta **1473**, 345–355

18 Matsuda, H., Kimura, S. and Iyanagi, T. (1999) Calmodulin activates intramolecular electron transfer between the two flavins of neuronal nitric oxide synthase reductase domain. In Flavins and flavoproteins (Ghisla, S., Kroneck, P., Macheroux, P. and Sund, H., eds.), pp. 171–174, Weber, Berlin

19 Daff, S., Sagami, I. and Shimizu, T. (1999) The 42-amino acid insert in the FMN domain of neuronal nitric-oxide synthase exerts control over Ca^{2+}/calmodulin-dependent electron transfer. J. Biol. Chem. **274**, 30589–30595

20 Klatt, P., Schmidt, K. and Mayer, B. (1992) Brain nitric oxide synthase is a haemoprotein. Biochem. J. **288**, 15–17

21 Munro, A. W., Noble, M. A., Robledo, L., Daff, S. N. and Chapman, S. K. (2001) Determination of the redox properties of human NADPH-cytochrome P450 reductase. Biochemistry **40**, 1956–1963

22 Noble, M. A., Munro, A. W., Rivers, S. L., Robledo, L., Daff, S. N., Yellowlees, L. J., Shimizu, T., Sagami, I., Guillemette, J. G. and Chapman, S. K. (1999) Potentiometric analysis of the flavin cofactors of neuronal nitric oxide synthase. Biochemistry **38**, 16413–16418

23 Miller, R. T., Martasek, P., Nishimura, J. S., Panda, S., Harris, D. E., Roman, L. J., Masters, B. S. and Kim, J.-J. P. (1999) The flavoprotein domains of nitric oxide synthase isoforms: site of possible regulatory control of flavin to heme electron transfer. In Flavins and flavoproteins (Ghisla, S., Kroneck, P., Macheroux, P. and Sund, H., eds.), pp. 151–154, Weber, Berlin

24 Miller, R. T., Martasek, P., Omura, T. and Masters, B. S. S. (1999) Rapid kinetic studies of electron transfer in the three isoforms of nitric oxide synthase. Biochem. Biophys. Res. Commun. **265**, 184–188

25 Gutierrez, A., Lian, L. Y., Wolf, C. R., Scrutton, N. S. and Roberts, G. C. (2001) Stopped-flow kinetic studies of flavin reduction in human cytochrome P450 reductase and its component domains. Biochemistry **40**, 1964–1975

26 Gutierrez, A., Doehr, O., Paine, M., Wolf, C. R., Scrutton, N. S. and Roberts, G. C. (2000) Trp-676 facilitates nicotinamide coenzyme exchange in the reductive half-reaction of human cytochrome P450 reductase: properties of the soluble W676H and W676A mutant reductases. Biochemistry **39**, 15990–15999

27 Oprian, D. D. and Coon, M. J. (1982) Oxidation-reduction states of FMN and FAD in NADPH-cytochrome P-450 reductase during reduction by NADPH. J. Biol. Chem. **257**, 8935–8944

28 Sem, D. S. and Kasper, C. B. (1994) Kinetic mechanism for the model reaction of NADPH-cytochrome P450 oxidoreductase with cytochrome *c*. Biochemistry **33**, 12012–12021

29 Sem, D. S. and Kasper, C. B. (1995) Effect of ionic strength on the kinetic mechanism and relative rate limitation of steps in the model NADPH-cytochrome P450 oxidoreductase reaction with cytochrome *c*. Biochemistry **34**, 12768–12774

30 Murataliev, M. B. and Feyereisen, R. (2000) Interaction of NADP(H) with oxidized and reduced P450 reductase during catalysis. Studies with nucleotide analogues. Biochemistry **39**, 5066–5074

31 Gachhui, R., Presta, A., Bentley, D. F., AbuSoud, H. M., McArthur, R., Brudvig, G., Ghosh, D. K. and Stuehr, D. J. (1996) Characterization of the reductase domain of rat neuronal nitric synthase generated in the methylotrophic yeast *Pichia pastoris* – Calmodulin response is complete within the reductase domain itself. J. Biol. Chem. **271**, 20594–20602

32 Viola, R. E., Cook, P. F. and Cleland, W. W. (1979) Stereoselective preparation of deuterated reduced nicotinamide adenine nucleotides and substrates by enzymatic synthesis. Anal. Biochem. **96**, 334–340

33 Pollock, V. V. and Barber, M. J. (2001) Kinetic and mechanistic properties of biotin sulfoxide reductase. Biochemistry **40**, 1430–1440

34 Barna, T. M., Khan, H., Bruce, N. C., Barsukov, I., Scrutton, N. S. and Moody, P. C. (2001) Crystal structure of pentaerythritol tetranitrate reductase: "flipped" binding geometries for steroid substrates in different redox states of the enzyme. J. Mol. Biol. **310**, 433–447

35 Brunner, K., Tortschanoff, A., Hemmens, B., Andrew, P. J., Mayer, B. and Kungl, A. J. (1998) Sensitivity of flavin fluorescence dynamics in neuronal nitric oxide synthase to cofactor-induced conformational changes and dimerization. Biochemistry **37**, 17545–17553

36 Miller, R. T., Martasek, P., Roman, L. J., Nishimura, J. S. and Masters, B. S. S. (1997) Involvement of the reductase domain of neuronal nitric oxide synthase in superoxide anion production. Biochemistry **36**, 15277–15284

37 Wolthers, K. R. and Schimerlik, M. I. (2001) Reaction of neuronal nitric-oxide synthase with 2,6-dichloroindolphenol and cytochrome c3+: influence of the electron acceptor and binding of Ca^{2+}-activated calmodulin on the kinetic mechanism. Biochemistry **40**, 4722–4737

38 Zhang, J., Martasek, P., Paschke, R., Shea, T., Masters, B. and Kim, J.-J. (2001) Crystal structure of the FAD/NADPH-binding domain of rat neuronal nitric-oxide synthase: comparisons with NADPH-cytochrome P450 oxidoreductase. J. Biol. Chem. **276**, 37506–37513

39 Wolthers, K. and Schimerlik, M. I. (2002) Neuronal nitric oxide synthase: substrate and solvent kinetic isotope effects on steady-state kinetic parameters for the reduction of 2,6-dichlorophenol and cytochrome c^{3+}. Biochemistry **41**, 196–204

Received 26 April 2002/14 June 2002; accepted 24 June 2002
Published as BJ Immediate Publication 24 June 2002, DOI 10.1042/BJ20020667